41th ERF, September 1–4, 2015, Munich, Germany

032

Optimized ERICA Engine Intake Wind Tunnel Test

G. Gibertini*[1], F. Auteri[1], L. Colaiuda[2], M. Ermacora[1], D. Grassi[1], and A. Zanotti[1]

[1]Politecnico di Milano – Dipartimento di Scienze e Tecnologie Aerospaziali
Via La Masa 34, 20156 Milano – Italy
[2]Revoind Industriale
Loc. Casale Marcangeli, 67063 Oricola (AQ) – Italy
e–mail: *giuseppe.gibertini@polimi.it

Keywords: Wind tunnel, Tilt-rotor, Endoscopic PIV, Directional probes.

Abstract

The present paper describes the experimental set up of the wind tunnel activity to assess the effectiveness of the CFD-based air-intake shape optimisation of the European platform tilt-rotor (ERICA). The wind tunnel campaign is carried out in the framework of the CleanSky TETRA project. The wind tunnel model was appositely designed and manufactured including the nacelle, the external wing and two interchangeable internal ducts (original and optimized). The performance evaluation is then made by the comparison of the pressure losses over the duct and the flow behavior at the engine face for both original and optimized intake duct shapes. Moreover, the evaluation of the internal flow field is made by means of an endoscopic PIV measurements performed in critical regions.

1 Introduction

Due to the expected growth of the rotorcraft traffic for passenger transport, the rotorcraft (including tilt-rotor) contribution to environmental impact, negligible today, would become more significant in next decade unless a major initiative succeeds in keeping it under control. An important aspect for the energy efficiency of an aircraft is the behavior of the engine air-intakes. Efficient aerodynamic design of air intakes is a challenging objective for airframe manufacturers since the inlet duct must be designed to act as a diffuser with gentile diffusion from flight Mach number to lower Mach number and higher values of static pressure. This leads to boundary layer instability as the flow is subjected to adverse pressure gradient. Moreover, an S-shaped duct is usually required for turbo-prop applications. A curved duct induces a secondary flow pattern, which essentially sets up a swirling flow at the duct exit [1]. Therefore, the internal shape of the curved duct should be designed in order to minimize total pressure loss and flow distortion at the AIP (Aerodynamic Interface Plane), which corresponds to the compressor's first stage of the full scale engine. This two performance parameters were taken into account by the GRC (Green Rotorcraft) consortium for the CFD-based shape optimisation of the air-intake duct of the European platform tilt-rotor (ERICA) [2].

The present paper describes the complete experimental set up developed in the frame of the Clean Sky TETRA project to evaluate the effectiveness of the intake duct shape optimization. The tests are carried out in the large wind tunnel (GVPM) of Politecnico di Milano (Polimi) on a scaled model which was specifically designed and manufactured for this project. The comprehensive experimental campaign includes both the original configuration and the optimised version.

The experimental activity includes different measurement techniques. A set of 128 pressure taps is obtained over both the ducts to obtain the static pressure distribution. Moreover, a detailed pressure mapping is made over the AIP using 5 directional probes which are fixed on a rotating frame that allows to perform a complete sweep of the AIP area. Also the directional probes are specifically made for this project and they were previously calibrated at Polimi aerodynamics laboratory. Lastly, an endoscopic PIV survey allows to evaluate the flow behavior in some critical points, mainly to assess the developement of a flow separation.

The paper describes in details the model design and manufacturing, the test rig and all the measurement systems involved in the wind tunnel test campaign.

2 Model Design

A scaled model (1:2.5) of the tilt-rotor ERICA nacelle and movable wing has been designed and manufactured by Revoind Industriale S.r.l. The choosed scale allows to center the hub axis with respect to the test chamber frontal area.

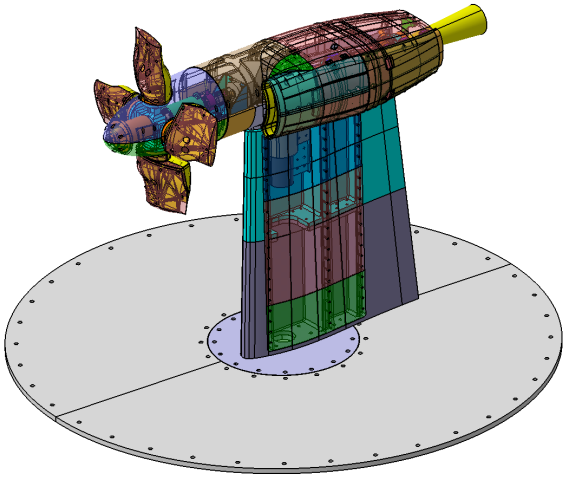

Figure 1: Overall scaled model.

The model consists of the following macro-items (see Figure 1):

- A movable wing divided in two parts, inner and outer;
- A tilting nacelle flanged to the wing;
- Two interchangeable intake ducts;
- A rotating hub provided with manually adjustable rotor blade stubs. Proper covers are also provided to be alternatively installed instead of rotor blade stubs to obtain a rotating hub clean geometry.

Moreover, the model includes two subsystems that are composed by an hydraulic motor and by 4 air-movers which provide, respectively, the hub rotation and the flow rate inside the intake duct.

The model was designed to allow for an easy assembly of movable parts, installation, check and repair/replacement of instrumentation. A FEM structural analysis was also performed in order to assess the margin of security against risks.

2.1 The air-intake model

The model design started from the original CAD drawings provided by GRC consortium, in which the external surface of the ERICA wing and nacelle is specified.

The wing trunk, representing the outer movable wing of the full scaled model, is made of 8 different items, as shown in Figure 2. Main parts are conceived as having full leading and trailing edge. Covers are designed to be connected to the main parts by means of screw fittings, so that it can be easily disassembled for instrumentation checks and/or repairs, and to easily set the relative pitch angle of wing and nacelle. The model will be installed in the test section by constraining the movable wing directly to the wind tunnel turn table, which allows to rotate the wing in order to reach the requested incidence angle.

The nacelle structure (see Figure 3) is designed in order to house the interchangeable duct systems to be tested, the rotor hub actuation system and the pressure measurement instrumentation. Valves and air-movers to manage both engine and by-pass flowsare located in the less intrusive and most efficient manner. Openings on the nacelle outer part are designed and manufactured in order to allow wind tunnel operations as changing air ducts to be tested, modifying relative attitude angle and accessing to the systems dedicated spaces (hydraulic motor, electric step motor, measurement instrumentation) for checks and/or repairs.

Figures 4 and 5 show the two main subsystems that take place inside the nacelle.

The intake ducts are entirely realized in aluminum and are designed in twenty items integrated by means of screws. A set of 128 steady

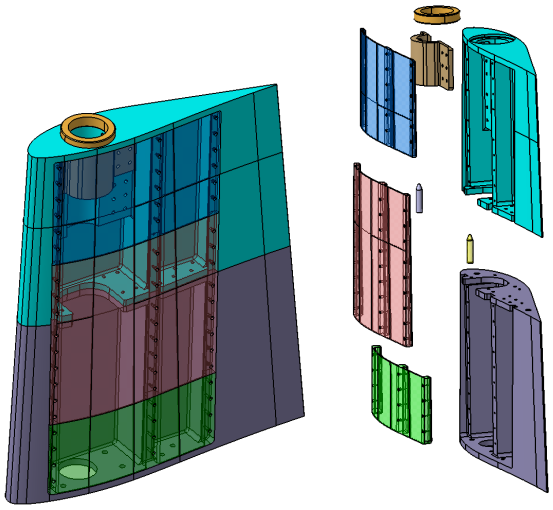

Figure 2: Wing model

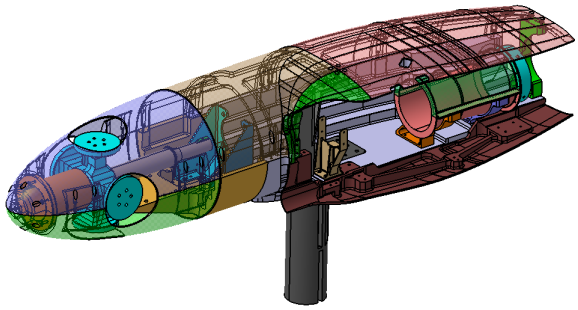

Figure 3: Nacelle Model without sub-assy components.

pressure taps is foreseen to map the internal static pressure distribution. Special care was taken in the handling of the sealing between air ducts and air pipes to avoid leakages. Moreover, 5 holes were made to allow the PIV instrumentation access. In fact, for each PIV acquisition, two endoscopes (one for the camera and one for the laser) are placed iside the duct. When the PIV instrumentation is removed, the holes are closed with proper covers shaped with the internal curvature of the duct.

The central part of the internal surface of the duct (S-shaped zone) is treated with a dark opaque paint aimed to minimize reflections of the laser during PIV measurements. The engine AIP section is instrumented with a motorized rotating frame supporting the 5 directional probes.

The rotor stub is realized in four items integrated by means of screws, following the aim

of weight saving in three design optimization phases. The stub attitude angle is set precisely by replacing five different stub links (see Figure 5) in order to obtain five different setting angles, as established for the different conditions to be tested. The test matrix foresees also a clean configuration (without stubs), so a joint cover is provided for this condition.

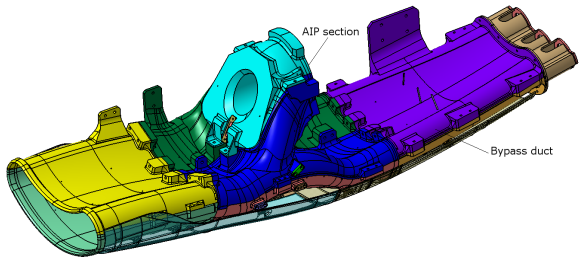

Figure 4: Intake duct model.

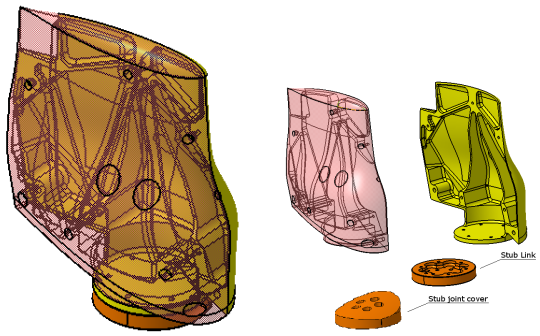

Figure 5: Stub model.

2.2 Air suction system

The wind tunnel is equipped with two different air pressure circuits that are feasible to be used in connection with two different types of air-movers. These air-movers enable to produce the necessary suction to assure the proper flow rate both in the AIP and in the by-pass ducts. As shown in Figure 6, one single air-mover is connected to the AIP by a proper connection pipe also having the function to minimize the flow distortion produced by the air-mover suction in correspondence of the AIP. On the by-pass duct, geometry and flow rate limitations induced to have a different solution that involves the use of 3 smaller air-movers.

These devices work exploiting the Coanda effect in order to produce a huge air flow with

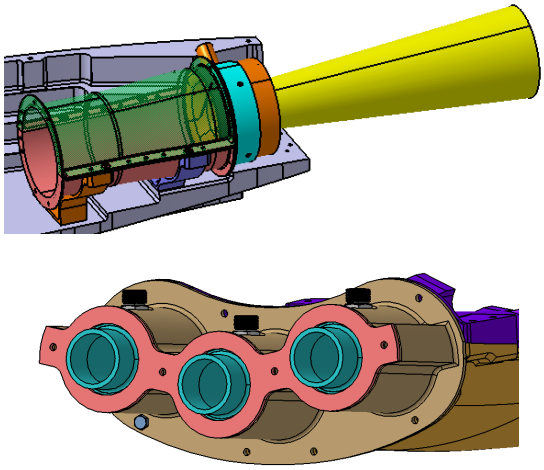

Figure 6: Air suction system.

the use of a small amount of compressed air. In fact, the suction produced by the air-mover generates a total flow that is 20 times greater than the compressed air flow used.

2.3 Rotating hub drive system

The rotary motion is provided to the hub by a Bosch Rexroth hydraulic motor, capable of providing the requested power in order to reach the maximum rotational hub speed planned for this test campaign. The transmission shaft is connected to the motor by a torsionally flexible joint (see Figure 7) and it is coupled to an incremental rotary encoder for a feedback control of the rotation. Both the shaft and the bearing cases are made of steel due to the high loads to which they are subjected. The two bearings that take place inside the case were choosed in order to manage both axial and radial loads.

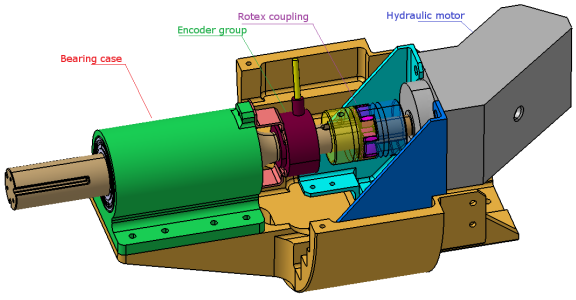

Figure 7: Drive and transmission system.

2.4 Structural analysis

Since the structural scheme of the whole wind tunnel model is macroscopically isostatic, a chain flow approach was used, starting from the load applied to the stubs (see the sketch in Fig. 8).

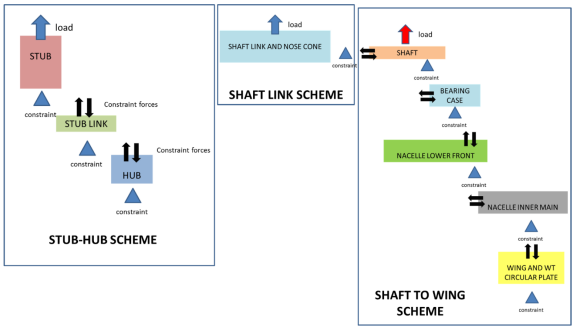

Figure 8: Structural analysis scheme.

For the load evaluation, both aerodynamic and inertial forces were taken into account. The angular acceleration was applied as inertia load on the concentrated masses of stubs and to the whole hub mass. The aerodynamic drag was calculated using the dynamic pressure obtained by vector composition of wind tunnel speed and tangential rotation speed at the tip of the stub. The drag coefficient was assumed equal to 1.2, a conservatively high value nearly to the one of a flat plate at incidence of 90°.

Following the specifications given by NASA [4], it was found that the critical condition is represented by the loss of a stub. In fact, the resultant unbalanced rotary system will introduce the highest loads to the model. All the analyses were then carried out under this scenario, applying a safety factor equal to 1.5. The margins of safety of the parts were calculated by using the highest Von Mises stress, whereas the screws verification were carried out using the maximum values of forces acting on them. Bearing calculation were made according to the methodology reported in Bruhn [5].

As an example, the results of the structural analyses obtained for the stub, the stub link and the connection flange of the nacelle with the wing are reported in Fig. 9.

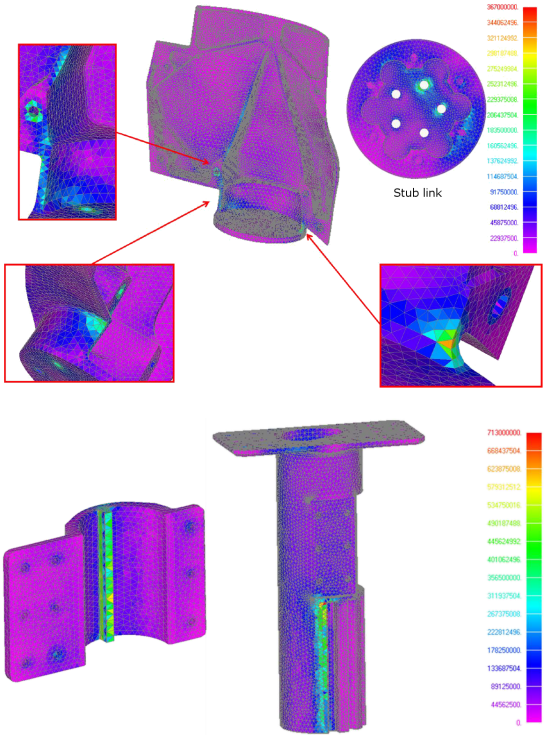

Figure 9: Von Mises stress analysis.

3 Experimental set up

The present section describes the test rig used for the wind tunnel tests carried out at GVPM. The wind tunnel closed test section is 6 m long, 4 m wide and 3.84 m high and the maximum wind velocity that can be reached is about 55 m/s with a free-stream turbulence level less than 0.1%. The feedback allowing an accurate velocity control is obtained by dynamic pressure measurement together with the measurement of thermodynamic quantities necessary to compute the fluid density.

3.1 Flow rate regulation system

The regulation of the flow-rate inside the intake duct is made by 2 different proportional servo-valves (the by-pass air-movers will be controlled simultaneously), that are used to control the flow of the compressed air that is brought to the air-movers.

The flow-rate evaluation, allowing the servo valve regulation, is obtained from velocity measurements carried out by means of an appropriate set of total pressure probes and wall pressure taps placed both in the by-pass duct

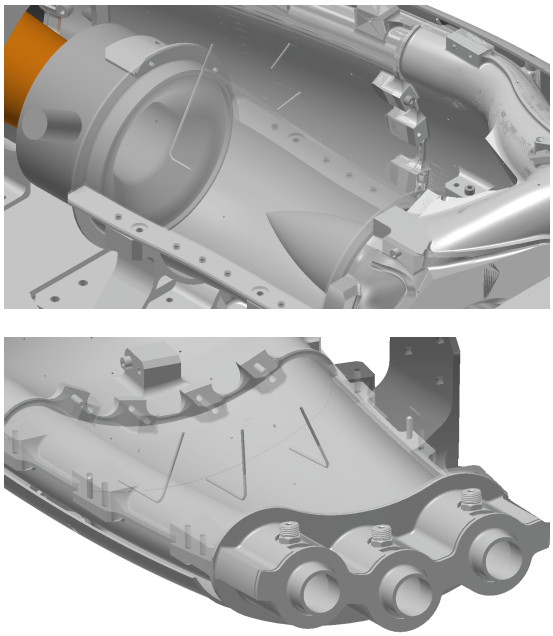

Figure 10: Total pressure probes for flow rate measurement.

and in the AIP connection pipe (see Fig. 10). This flow-rate measurement system is previously calibrated using a custom-made Venturi tube, that could be directly coupled to the intake inlet section. The result of the calibration is a look-up table that directly links the flow-rate to the velocity measurement and can be used during the tests to easily set the requested flow rate.

3.2 Static pressure measurements

The intake duct is designed including 128 pressure taps, on which a steel tube with an internal diameter of 0.31 mm is fitted. Figure 11 shows the pressure taps position on the model. The pressure measurements points are not uniformly spaced as, following the results of the CFD simulations carried out by Garavello *et al.* [2], it has been chosen to reduce the space between the taps in the regions that present stronger gradients.

Each steel tube is properly connected by a plastic tube to an ESP miniature pressure scanner placed inside the nacelle. The employed scanners are miniature electronic differential pressure measurement units consisting of an array of silicon piezoresistive pressure sensors, one for each pressure port. A total number of

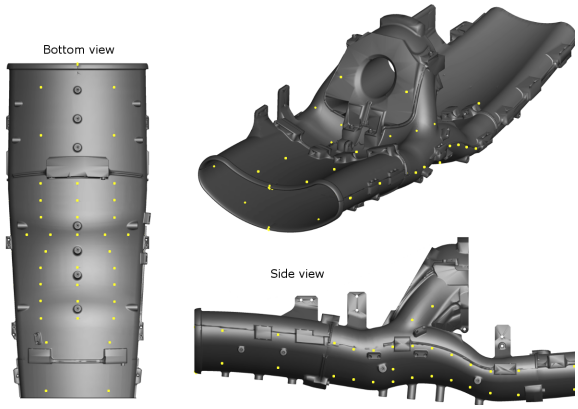

Figure 11: Static pressure taps distribution.

four scanners (each with 32 pressure inputs) are dedicated for the static pressure measurements over the intake. The scanners are connected to a DTC Initium data acquisition system which integrates an advanced analog circuit design with innovative Digital Temperature Compensation (DTC) technology to maintain optimal accuracy without on-line span calibration.

3.3 Total pressure and flow distortion measurement

A proper set of directional probes is made in order to provide information about the flow distortion as well as to survey the total pressure distribution among the AIP. In particular, it consists on three 5-hole probes and two 3-hole probes arranged on different radial positions, as can be seen in Fig 12. Each probe is manufactured by bending different stainless steel tubes with an external diameter of 0.8 mm and internal diameter of 0.4 mm. In order to reduce the Reynolds number dependence, the tubes are cut with an angle of 45°. The probes are connected to a rotating frame that is controlled by a stepper motor which allows a precise handling of the entire system. In particular, this frame is used for a rotational sweep with an angular step of 22.5°, so that a global amount of 80 measurement points over the AIP is acquired. During the experimental campaign all the probes are connected to a different scanner system (of the same type as the ones connected to the duct pressure taps) located inside the nacelle.

The probes specifically manufactured for

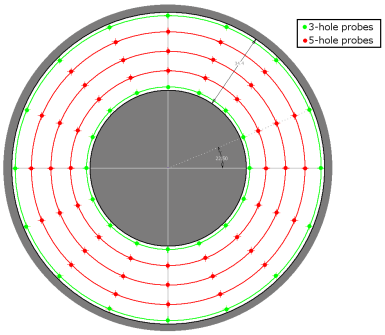

Figure 12: Distribution of the measurement points at the AIP.

these tests were previously calibrated at the Aerodynamics Laboratories of Polimi. The calibration tests were performed under monitored conditions in a wind tunnel with 150×200 mm test section that can reach a maximum speed of 100 m/s. The rotation of the probes in pitch and yaw directions was controlled by two stepper motors that command the movement of the entire probe supporting structure.

For the present calibration tests a three dimensional curve-fits was performed over the entire set of calibration points. This technique compensates the eventual non-simmetry of the probes and smooths out the effects of bad data points. A range of angles between $-25°$ and $+25°$ was considered for both pitch and yaw during the calibration of the probes. An accuracy evaluation was made by direct comparison of the measurements obtained with the probes at known conditions. An overall good accuracy was obtained with an estimated maximum error of 1° for angle reconstruction and 2% of the free-stream velocity for velocity evaluation.

3.4 Particle Image Velocimetry

The PIV system consists of a Litron NANO-L-200-15 Nd:Yag double pulsed laser with a 200 mJ output energy and a wavelength of 532 nm, and an Imperx ICL-B1921M CCD camera with a 12 bit, 1952 × 1112 pixel array. The synchronization of the emission of the two laser pulses with the camera exposure of the image pairs is controlled with a 6 channel Quantum Composer QC9618 pulse generator. The seeding is supplied by a PIVpart30 particles generator by PIVTEC featuring Laskin atomizer nozzles. The seeding consists in small oil droplets with diameter in the range of 1-2 μm. The Polimi PIV system is also suitable for endoscopic investigation. For this purpose a rigid boroscope and a Dantec endoscopic illuminator are employed. Since the area of interest is quite small, the boroscope is coupled with a optical reducer that restricts the field of view, allowing to have an higher image resolution. The endoscopic illuminator produces the laser sheet inside the investigation area and is coupled with the laser light source by means of a light arm that allows an easier positioning of the illuminator. Both endoscopic instruments (the boroscope and the illuminator) have a diameter of 8 mm and can be equipped with a 45° mirror to produce a 90° degrees deflection of the vision or illumination direction. The hub shaft encoder signal is used to trigger the PIV images acquisition with a prescribed azimuthal position of the blade during the test. The software for images evaluation is PIVview 2C/3C [6] developed by PIVTEC in close cooperation with the PIV-Groups of the German Aerospace Center (DLR). The PIVview software is a complete PIV evaluation program including advanced processing algorithms as multiple-pass and multiple-grid methods, image deformation methods, various peak detectors and fitting algorithms, ensemble correlation, classical and non-linear peak detection and a good image pre-processing tool [7].

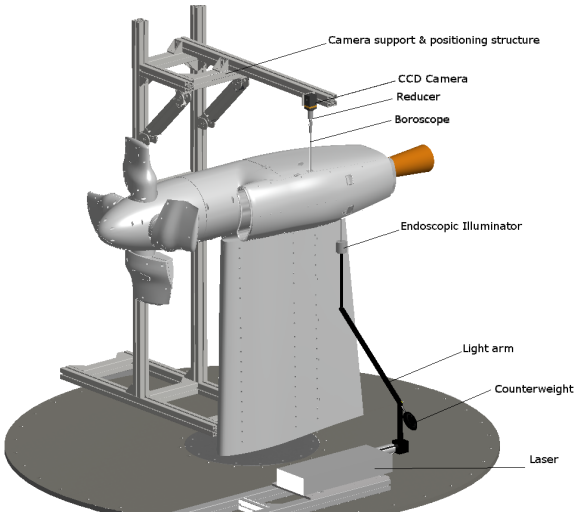

Figure 13: PIV instrumentation layout.

The complete PIV setup is shown in Fig. 13.

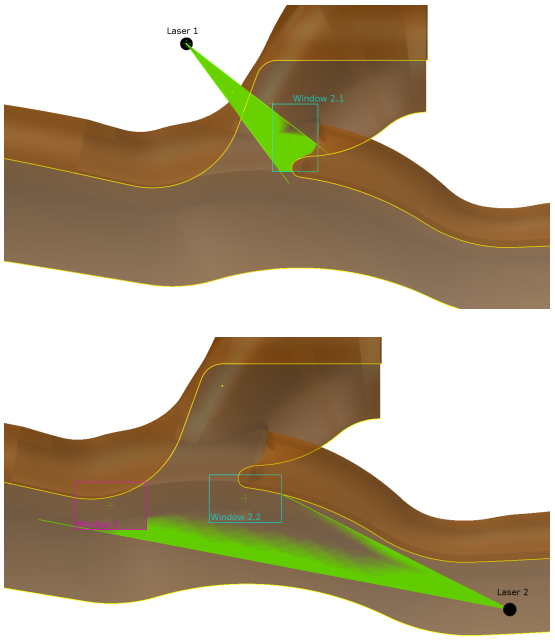

Figure 14: Detail of the PIV field of view.

As the conditions selected for PIV surveys are only in hovering, i.e. without wind inside the test section, the camera can be supported by an external dedicated structure, that allows the positioning in space. The laser is placed on the wind tunnel floor as the light ray is properly guided using an articulated mirror arm, which didn't require a particular support.

In particular the flow behavior is checked in two critical positions (see Fig. 14), in order to investigate the effect of the duct optimized geometry on flow separation. To provide the correct illumination to both windows it is necessary to split window 2 in two parts. The model is designed so that there are three different holes for the camera boroscope entries and two holes for the laser endoscope illuminator. As can be seen, the "laser 1" position is outside the duct and the illumination is guaranteed by a transparent element placed on the duct surface.

4 Conclusions

An experimental test rig for the assessment of the CFD-based optimization of the air-intake duct of the ERICA tilt-rotor was designed and set up for wind tunnel tests. The air-intake model was designed including the nacelle, the external wing and two interchangeable internal ducts (original and optimized). A structural analysis of the model does not show criticity taking into account the loads evaluated for the scheduled wind tunnel test conditions. Different measurement techniques are employed to evaluate the effects of the optimized duct geometry by comparison with the original configuration. In particular, the comprehensive test campaign includes static pressure measurement on the duct surface, directional probes measurements at the AIP and the use of endoscopic PIV.

5 Acknowledgements

References

[1] Seddon J., Understanding and countering the swirl in S-ducts: tests on the sensitivity of swirl to fences, *Aeronautical Journal, R.Ae.Soc.*, 1984.

[2] Garavello A., Benini E., Ponza R., Scandroglio A. and Saporiti A., Aerodynamic Optimization of the ERICA Tilt-Rotor Intake and Exhaust System, *37th European Rotorcraft Forum*, Ticino Park, Italy, 13-15 September, 2011.

[3] Nannoni F., Giancamilli G. and Cicalé M., ERICA: the european advanced tiltrotor, *27th European Rotorcraft Forum*, Moscow, Russia, 11-14 September, 2001.

[4] Wind-tunnel model systems criteria, LPR 1710.15, NASA Langley Research Center, July 22, 2004.

[5] Bruhn E. F., Analysis and design of flight vehicle structures, , Tri-State Offset Company ed.

[6] PIVview 3C version 3.0, User Manual, PIVTEC, www.pivtec.com.

[7] Raffel M., Willert C. and Kompenhans J., Particle Image Velocimetry, a practical guide, Springer, Heidelberg, 1998.